Mode-splitting-based optical label-free biosensing with a biorecognition-covered microcavity

Xu Yi, Yun-Feng Xiao, Yin Feng, Dong-Ying Qiu, Jing-Yi Fan, Yan Li, and Qihuang Gong

Citation: Journal of Applied Physics **111**, 114702 (2012); doi: 10.1063/1.4725424
View online: http://dx.doi.org/10.1063/1.4725424
View Table of Contents: http://scitation.aip.org/content/aip/journal/jap/111/11?ver=pdfcov
Published by the AIP Publishing

Mode-splitting-based optical label-free biosensing with a biorecognition-covered microcavity

Xu Yi, Yun-Feng Xiao,[a] Yin Feng, Dong-Ying Qiu, Jing-Yi Fan, Yan Li, and Qihuang Gong
State Key Laboratory of Mesoscopic Physics, Department of Physics, Peking University, Beijing 100871, People's Republic of China

(Received 29 September 2011; accepted 10 May 2012; published online 7 June 2012)

A pair of counter-propagating high-Q whispering-gallery modes (WGMs) can couple to each other and produce two new modes with a significant resonance splitting when single or multi-Rayleigh scatterers are adsorbed on the microcavity surface. In this paper, we investigate the mode-splitting-based biosensing by using a biorecognition-covered WGM microcavity because the pre-covering is essentially necessary for label-free detection of specific biological targets. It is shown that the quantitative detection, e.g., nanoparticle sizing, is strongly affected by the biorecognition, and the minimum target size suitable for detection is subjected to the surface pre-covering ratio. To eliminate this degradation induced by biorecognition, we further propose to use the total linewidth broadening of the two new modes as the detection signal, which is immune to thermal fluctuation. © *2012 American Institute of Physics*. [http://dx.doi.org/10.1063/1.4725424]

I. INTRODUCTION

Label-free optical biosensors based on microresonators (namely, microcavities) have attracted much attention over the past few years because they hold potential in biomedical research, healthcare, pharmaceuticals, environmental monitoring, and homeland security.[1–10] Among them, whispering-gallery mode (WGM) microresonators are of special interests owing to their ultra-high Q-factors, small mode volumes and ease for mass production on a chip. So far, the ultrahigh sensitivity down to a single-particle level has been demonstrated through monitoring the shift of the resonance frequency, which is induced by single particles (e.g., Influenza A virions) bound on the resonator surface.[11,12] Unfortunately, this ultrasensitive detection is very fragile to the environment temperature fluctuation and the probe laser induced noises. Recently, based on the targets-induced Rayleigh scattering in a high-Q WGM microcavity, a self-referenced detection has been developed and applied to nanoparticle sizing[13–18] and orientation detection.[19] Specifically, this method utilizes the mode splitting as the detection signal and it is immune to the thermal fluctuations of environment and random binding positions of the targets.[20] Therefore, it provides a promising alternative method for highly sensitive optical biosensing.

In realistic optical microcavity biosensors, the label-free nature originates from the fact that the biorecognitions are pre-covered on the surface of microresonators, and they specifically bind the biological targets.[21,22] For the mode shift mechanism, the pre-covering mainly causes a resonance frequency shift. Thus, by resetting the zero point of the signal, the accurate detection of the biological targets can be realized in principle. However, for biosensors based on the mode-splitting mechanism as mentioned above, the pre-covering may arouse a more complex situation, because the biorecognition on the microcavity surface also produces Rayleigh scattering. Moreover, the magnitude of frequency splitting does not monotonously increase (in some cases, it may even decrease) with more and more nanoparticles binding on microcavity,[14,23,24] and this cannot be removed by simply setting the zero point of the detection signal.

In this paper, using the analytical result presented in Ref. 14 and Monte Carlo simulation method, we theoretically analyze the mode-splitting-based label-free biosensing with the biorecognition on the cavity surface. We show that apart from biological target, the biorecognition would also induce the mode splitting which could degrade the quantitative measurement, such as the sizing of targets. To eliminate this degradation induced by biorecognition, here, we propose to use the total linewidth broadening as the sensing signal, which is immune to thermal noises but depends on the binding position of the targets.

II. THEORETICAL MODEL

Before the analysis in the presence of biorecognition on the microcavity surface, we briefly review the mode splitting mechanism in a high-Q WGM microcavity. WGM cavity supports a pair of counter-propagating high-Q modes (clockwise (CW) and counter-clockwise (CCW) modes) with the degenerate resonance wavelength and linewidth. When biomolecules or nanoparticles are adsorbed on cavity surface, the two travelling WGMs will couple to each other due to the Rayleigh scattering effect.[25–30] This coupling lifts the degeneration and forms two new modes with the split resonance frequencies and distinct linewidths. In a realistic experiment, the probe light is coupled into the microcavity through a fiber taper. In the absence of nanoparticles, the transmission spectrum is a single Lorentzian lineshape dip; while in the presence of nanoparticles, the spectrum may exhibit a doublet structure as a result of the mode splitting.

The splitting induced by multi-Rayleigh-scatterer could be theoretically studied with full quantum theory with dipole approximation.[14,26] Two key parameters are used to describe

[a]Author to whom correspondence should be addressed. Electronic mail: yfxiao@pku.edu.cn. URL: http://www.phy.pku.edu.cn/~yfxiao/index.html.

the coupling of the modes induced by the n-th scatterer: the coupling strength between the two counter-propagating cavity modes expressed by $g_n f^2(\theta_n)$, and the scattering loss induced by the scatterer expressed by $\Gamma_n f^2(\theta_n)$. Here $f(\theta_n)$ is the mode function defined as the field intensity at the n-th molecule's position normalized by the maximum field intensity in cavity; θ_n is defined in Fig. 1(a). Using Weisskopf-Wigner semi-QED (Quantum Electrodynamics) treatment,[14,26] we obtain $g_n = -\alpha_n \omega_0 / 2V_c$, $\Gamma_n = \alpha_n^2 \omega_0^4 / 6\pi v^3 V_c$, where α_n, v, and V_c represent the polarization intensity of the n-th scatterer, the light speed in the surrounding environment, and the cavity mode volume. In the situation that both the biorecognition molecules and biological targets are attached on the cavity surface, the frequency shifts and linewidth broadenings of the two new eigenmodes can be calculated. For convenience, here we denote one mode as "+," while the other as "−." Their resonant frequencies, linewidths, frequency shifts, linewidth broadenings, resonant frequency splitting, and linewidth difference are represented as $\omega_\pm$, $\gamma_\pm$, $g_\pm$, $\Gamma_\pm$, $\Delta g_\pm$, and $\Delta\Gamma_\pm$. Suppose there are N_b biorecognition molecules and N_t biological targets on the cavity surface, and the mutual polarization among molecules is small and negligible in liquid environment,[14] the parameters mentioned above can be expressed as[14]

$$g_\pm \equiv \omega_\pm - \omega_0 = \pm \mathrm{Re}(\eta g_s^*) \pm \frac{1}{2}\mathrm{Im}(\eta \Gamma_s^*) + \sum_{n=1}^{N_b+N_t} g_n f^2(\theta_n), \quad (1)$$

$$\Gamma_\pm \equiv \gamma_\pm - \gamma_0 = \pm \mathrm{Re}(\eta \Gamma_s^*) \pm 2\,\mathrm{Im}(\eta g_s^*) + \sum_{n=1}^{N_b+N_t} \Gamma_n f^2(\theta_n), \quad (2)$$

$$\Delta g_\pm \equiv |g_+ - g_-| = |2\,\mathrm{Re}(\eta g_s^*) + \mathrm{Im}(\eta \Gamma_s^*)|, \quad (3)$$

$$\Delta\Gamma_\pm \equiv |\Gamma_+ - \Gamma_-| = |2\,\mathrm{Re}(\eta \Gamma_s^*) + 4\,\mathrm{Im}(\eta g_s^*)|, \quad (4)$$

where ω_0 and γ_0 are the resonance frequency and linewidth of the bare cavity mode, respectively. For simplicity, we have defined $g_s \equiv \sum_{n=1}^{N_b+N_t} g_n f^2(\theta_n) e^{2ikx_n}$, $\Gamma_s \equiv \sum_{n=1}^{N_b+N_t} \Gamma_n f^2(\theta_n) e^{2ikx_n}$, and $\eta \equiv \sqrt{(ig_s + \Gamma_s/2)/(ig_s^* + \Gamma_s^*/2)}$, with k being the wave vector, and x_n the location of the n-th scatter (including the biorecognition molecules and targets) along the principle diameters.

The transmission of the fiber taper, defined as the ratio of the output and the input intensity, can be calculated through standard cavity input-output relation

$$T = \frac{I_{\mathrm{out}}}{I_{\mathrm{in}}} = \left| 1 - \frac{\kappa_1}{2} \sum_{q=+,-} \frac{1}{i(\omega_0 - \omega + g_q) + (\kappa_0 + \kappa_1 + \Gamma_q)/2} \right|^2, \quad (5)$$

where ω is the angular frequency of the input light; κ_0 and κ_1 represent the intrinsic damping rate and the taper-cavity coupling strength, respectively. Equations (1)–(4) could be further simplified if only one species of nanoparticle (either biorecognition molecules or biological targets) are on cavity surface. In this case, we have $g_n = g_0$ and $\Gamma_n = \Gamma_0$ for each scatterer, and Eqs. (1)–(4) could be re-expressed as

$$g_\pm = \sum_{n=1}^{N} g_0 f^2(\theta_n) \pm g_0 \left| \sum_{n=1}^{N} f^2(\theta_n) e^{2ikx_n} \right|, \quad (6)$$

$$\Gamma_\pm = \sum_{n=1}^{N} \Gamma_0 f^2(\theta_n) \pm \Gamma_0 \left| \sum_{n=1}^{N} f^2(\theta_n) e^{2ikx_n} \right|, \quad (7)$$

$$\Delta g_\pm = 2 \left| \sum_{n=1}^{N} g_0 f^2(\theta_n) e^{2ikx_n} \right|, \quad (8)$$

$$\Delta\Gamma_\pm = 2 \left| \sum_{n=1}^{N} \Gamma_0 f^2(\theta_n) e^{2ikx_n} \right|, \quad (9)$$

where $N = N_b$ or N_t. With the results above, we are able to analyze the characteristics of transmission spectra in the presence of biorecognition on an ultra-high Q microtoroid cavity surface in liquid environment. The major (minor) diameter of the microtoroid used here is 80 (5) μm and the corresponding mode volume in 680-nm wavelength is about 330 μm^3. $f(\theta_n)$ can be obtained through numerical simulation (Fig. 1(a)), $f^2(\theta_n) = 0.2039 \times \exp(-0.0018\,\theta_n{}^2)$. These parameters are used throughout this paper unless specified.

III. MODE SPLITTING INDUCED BY BIORECOGNITION MOLECULES

Label-free nature of an optical WGM sensor is dependent on biorecognition (e.g., antibodies) pre-covered on the microcavity surface, which ensures binding with the specific biological targets. As mentioned above, for biosensors based on the mode splitting, the pre-covered biorecognition molecules on the cavity surface may induce the additional splitting and may degrade the detection signal of biological targets. In an ideal situation, the surface of cavity would be entirely covered with a layer of antibodies and no splitting

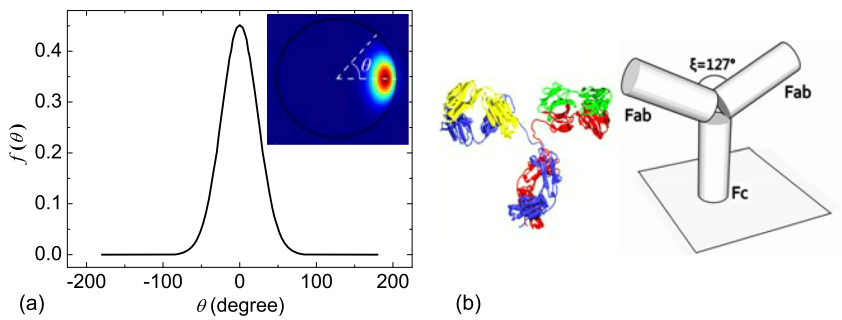

FIG. 1. (a) Mode function depending on the angle θ defined in the inset. Inset: Cross-section mode distribution of a fundamental TE mode obtained from numerical simulation. (b) Three-dimensional structure and a simplified model of IgG antibody. The length of each rod is about 8 nm, and the diameter is 3 nm. The average angle between the two Fabs is 127°.

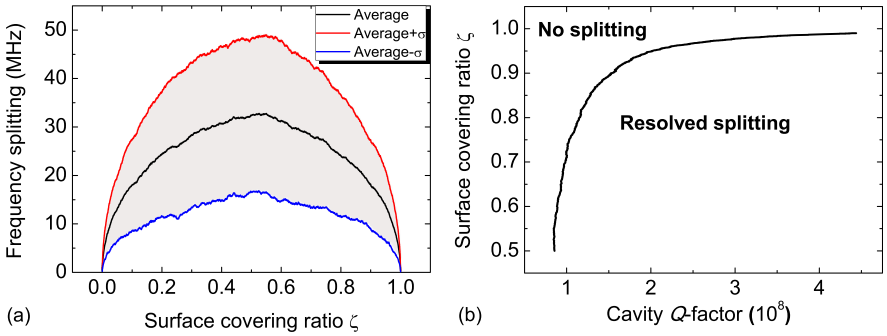

FIG. 2. (a) Frequency splitting induced by the antibody vs. the surface covering ratio ζ, where σ is the standard deviation. (b) Critical cavity Q-factor for different surface coating ratio. In the upper left area of the curve, no splitting appears before adsorption of biological targets, while in the lower right area, a mode splitting is resolved after antibody coating procedure.

will be observed, because the antibodies exert the same influence on modes + and − (i.e., modes + and − experience the same shifts and line broadenings). However, in a real situation, the cavity surface cannot be entirely covered due to the imperfectness of the technique.[31,32] Thus, this imperfectness may result in mode splitting phenomenon before the binding of the biological targets. Moreover, even if no splitting is resolved after pre-covering process, the pre-covering innately affects the quantitative detection signal, as depicted in Eqs. (1)–(4). In the following, we quantitatively study the influence of the pre-covering with Monte Carlo simulation method.

Here, we consider a specific antibody molecule IgG. Its three dimensional structure can be treated as a combination of three nanorods with refraction index about 1.50, as shown in Fig. 1(b). The length l of each rod is proximately 8 nm and the diameter d is about 3 nm. The angle ξ between the two Fabs is different for each type of IgG, and here we take IgG2 as an example, whose ξ is 127° on average.[33] In a common pre-covering process, antibodies are randomly located on the surface, with the Fc attached to the cavity due to the specific affinity force, enabling the Fabs to catch specific antigens. In liquid environment with refraction index of 1.33, g_n and Γ_n of the antibody can be obtained analytically with boundary conditions of the electric field.[19] For transverse electric (TE) mode, $g_n/2\pi = g_0/2\pi = 0.024$ MHz and $\Gamma_n/2\pi = \Gamma_0/2\pi = 0.187$ Hz; while for transverse magnetic mode, $g_n/2\pi = g_0/2\pi = 0.023$ MHz and $\Gamma_n/2\pi = \Gamma_0/2\pi = 0.172$ Hz. In this calculation, mutual polarization between rods has been neglected, as it is much smaller than the polarization of an individual rod.[14]

Considering the random positions of biorecognition molecules, here we use Monte Carlo simulation to study the system. Approximately, the maximum number of antibodies of a layer on cavity surface N_0 can be represented by the ratio between cavity surface area and the cross-section area of molecules, and we have $N_0 \sim \pi^2 \times 80 \times 5\,\mu m^2/(2l)^2 = 1.542 \times 10^7$. Then we generate N_b ($<N_0$) random positions of antibodies, marked by x_n and θ_n. These values are sequently inserted into Eqs. (6)–(9) to derive the magnitude of frequency splitting and linewidth broadening. In order to obtain statistically reliable results, this step is repeated for 500 times and the average magnitudes can be obtained.

Figure 2(a) presents how the frequency splitting of a fundamental TE mode depends on the pre-covering ratio ζ (defined as $\zeta = N_b/N_0$) on average. It can be found that the splitting reaches its maximum around $\zeta = 0.5$, and decreases to zero when ζ approaches 0 or 1, as expected. The decrease at $\zeta > 0.5$ is caused by the fact that the newly adsorbed molecules are likely to compensate the splitting induced by previous molecules when ζ is large. This result suggests that to avoid large mode splitting in coating process, one need either large ($\zeta > 0.5$) or small ($\zeta < 0.5$) covering ratio. Considering ζ is proportional to the number of binding spots for the biological targets, a large ζ is beneficial to the fast response of the highly sensitive biosensing.

The pre-coating induced frequency splitting may result in the observable split modes in the transmission spectra. Here, we neglect the scattering and absorption losses from the pre-coated biorecognition molecules as they are much smaller than the intrinsic loss of the WGM, which will be discussed in the following. As shown in Fig. 2(b), the resolved splitting depends on both the pre-coating ratio ζ and the intrinsic Q factor of the WGM. In the upper left region, no splitting is resolved because of either a small splitting or a large intrinsic linewidth. In the lower right region, splitting is observable because the splitting exceeds the cavity linewidth. For instance, when $\zeta = 0.5$, we obtain $\Delta g_{\pm}/2\pi = 5.16$ MHz. In this case, the mode splitting phenomenon appears for cavity with Q-factor higher than 8.6×10^7. According to the simulation, the Q factor could reach 6×10^8 for the cavity geometry described in this paper, and Q-factor as high as 10^8 has been demonstrated in Refs. 12 and 34.

Apart from mode splitting, this pre-covering also causes red shifts of the resonance wavelengths and lowers the Q factors of the two new modes. First, this red shift effect can be evaluated by calculating $(g_+ + g_-)/2$. The magnitude of red shift is proportion to ζ and reaches its maximum of 13 pm at $\zeta = 1$. Second, the Q factors are lowered due to the scattering and absorption losses induced by the biorecognition molecules. The scattering loss is evaluated with $(\Gamma_+ + \Gamma_-)/2$ and can be derived from Eq. (7). The absorption loss of antibody is estimated from the experiment result in Ref. 35, which shows $\mathrm{Im}\{\alpha\}$ is about $1/4 \times 10^{-4}$ $\mathrm{Re}\{\alpha\}$ for protein in 680 nm wavelength band. Both the scattering and absorption losses increase linearly with ζ, and approach their maxima at $\zeta = 1$. At $\zeta = 1$, the Q factors related to the scattering and absorption losses are $Q_{\mathrm{scattering}} = 6.4 \times 10^9$ and $Q_{\mathrm{absorption}} = 1 \times 10^9$. Thus, both $Q_{\mathrm{scattering}}$ and $Q_{\mathrm{absorption}}$ are one-order-of-magnitude larger than the typical Q factor of the WGMs in liquid environment ($Q \sim 10^8$)[12,36] and play a minor effect on the mode linewidth.

IV. NANOPARTICLE SIZING IN THE PRESENCE OF THE BIORECOGNITION

Quantitative measurement down to the single biological target level is of interest in optical biosensors. Therefore, an important issue is whether the quantitative detection, such as biological target sizing, is feasible with the presence of the biorecognition. Here, we consider the detection of a single spherical virus, whose surface has specific protein. The radius of the virus is typically tens of nanometers. In the detection, the radius r of the spherical viral nanoparticle can be calculated from the sensing signal $\Delta\Gamma_{\pm}/\Delta g_{\pm}$, which is immune to the particle position and the environment fluctuation.[13,20] Here, $\Delta\Gamma_{\pm}/\Delta g_{\pm} = \alpha_0(\omega_0^3/3\pi v^3)$, and $\alpha_0 = 3(\varepsilon_2 - \varepsilon_1)V/(\varepsilon_2 + 2\varepsilon_1)$, with $V = 4\pi r^3/3$ being the volume of viral nanoparticle, and ε_1 (ε_2) the relative permittivity of the surrounding environment (the viral nanoparticle).

We now quantitatively analyze the detection in the presence of the pre-covered biorecognition. Due to carousel effect,[37] we could assume that a single spherical target viral nanoparticle with refractive index 1.50 is attached to the position with the maximum field intensity ($\theta = 0$ and random x location along the principle diameters). Under these conditions, $\Delta\Gamma_{\pm}/\Delta g_{\pm}$ can be obtained, from which we can derive the radius of the viral nanoparticle. It should be noted that the measured radius is subjected to position x, because the mode distribution is determined by both biorecognition and target viral nanoparticle. Thus, by generating 3600 random values to x, we calculate the measured radius for 3600 times and obtain its average value (Fig. 3(a)) and relative standard error (Fig. 3(b)). In Fig. 3(a), it is found that for a small viral nanoparticle, the measured average radius deviates greatly from the actual value. This is because the coupling strength (i.e., the splitting) between CW and CCW modes is dominated by the biorecognition molecules. While for a large target viral nanoparticle (e.g., $r > 30$ nm), the biorecognition molecules play a minor role in the target nanoparticle splitting, and the error can also be suppressed to an acceptable level. For example, when $\zeta = 0.5$, the errors below 10% (5%) are achieved when the radius of the biological target is larger than 40 nm (50 nm). The error could be further lowered through increasing pre-covering ratio as shown in dash dotted ($\zeta = 0.7$) and short dashed ($\zeta = 0.9$) curves in Fig. 3(b), because a large pre-covering ratio can significantly reduce the biorecognition induced mode splitting. Lowering the pre-covering ratio from $\zeta = 0.5$ could also decrease the splitting induced by biorecognition and suppress the error, but meanwhile it would reduce the number of binding spots for biological target and lower the detection efficiency, as well as the response. Furthermore, when the particle is not attached at the equatorial region (the position with the maximum field intensity), the relative error of the detection increases as the splitting induced by the biological target decreases.

V. DISCUSSIONS

In the above section, we have shown that the detection signal composed of $\Delta g_{\pm}$ and $\Delta\Gamma_{\pm}$ is degraded by the biorecognition, especially for the detection of small biological targets. This is because both $\Delta g_{\pm}$ and $\Delta\Gamma_{\pm}$ depend on biorecognition and its impact cannot be removed by resetting the zero point of signals. The underlying physics is that the biorecognition not only causes a splitting before the biological targets detection but also contributes to the mode distribution during the detection.[14,23]

To entirely eliminate this degradation induced by biorecognition, we revisit Eqs. (1) and (2) and find that it is hard to distinguish the effects related to the biorecongnition and biological targets. However, they can be decoupled if we define the total linewidth broadening $\Gamma_+ + \Gamma_- = \sum_{n=1}^{N_b} 2\Gamma_n f^2(\theta_n) + \sum_{n=1}^{N_t} 2\Gamma_n f^2(\theta_n)$ or the total shift $g_+ + g_- = \sum_{n=1}^{N_b} 2g_n f^2(\theta_n) + \sum_{n=1}^{N_t} 2g_n f^2(\theta_n)$ of the two modes as the detection signal. In other words, the impact of the biorecognition can be principally removed by resetting the zero point of the signal. Furthermore, it should be noted that only the total linewidth broadening $\Gamma_+ + \Gamma_-$ is immune to the thermal fluctuation of the environment. Nevertheless, the linewidth broadening still depends on the binding positions of the targets. In Ref. 38, Zhu *et al.* used the signal $S = (\Gamma_+ + \Gamma_-)/(g_+ + g_-)$ to remove the effect of binding positions of the target and detect the size of the target, but this signal is no longer immune to the thermal fluctuation of the environment.

We provide more remarks on the measurement of the total linewidth broadening. In general, the binding of biological targets not only results in the mode splitting and the scattering loss but also produces the additional absorption loss for the WGM, which contributes to the total linewidth broadening. Considering that the absorption loss is represented by the imaginary part of resonance frequency, its contribution can be expressed as $\Gamma_{\text{abs}} = \sum_{n=1}^{N_t} 4f^2(\theta_n)\text{Im}\, g_0$. Based on this, we can estimate the effect of the target absorption. Here, we neglect the complexity of absorption spectra and

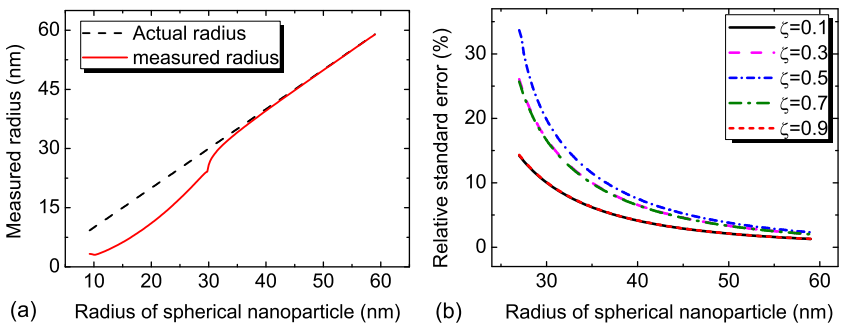

FIG. 3. (a) Measured radius of spherical nanoparticle vs. actual radius when the pre-covering ratio $\zeta = 0.5$. (b) Relative standard error for nanoparticle sizing depending on its radius and the different surface covering ratio ζ.

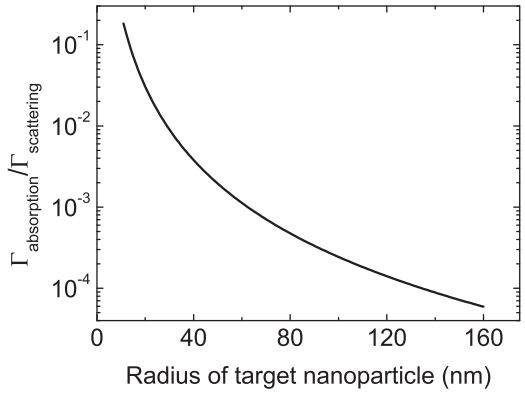

FIG. 4. Ratio of linewidth broadening induced by absorption and scattering losses depending on the radius of target nanoparticle.

take $\mathrm{Im}\{\alpha\} \sim 1/4 \times 10^{-4}\ \mathrm{Re}\{\alpha\}$ (Ref. 35) for simplicity but without losing the underlying physics. Figure 4 presents the comparison between $\Gamma_{scattering}$ and $\Gamma_{absorption}$ for a single biological target with the different sizes. In principal, when the radius of biological targets is larger than 30 nm, the absorption loss is smaller than the scattering loss by two orders of magnitude.

VI. SUMMARY

In summary, we have theoretically investigated the mode-splitting-based biosensing in the presence of biorecognition molecules. We demonstrate that the minimum size of biological targets suitable for detection is strongly affected by the biorecognition molecules. For instance, the relative standard error for sizing single target nanoparticle exceeds 30% when the radius of the target is about 30 nm. To remove the effect resulted from the biorecognition, we further propose to apply the total linewidth broadening of the two split modes as the sensing signal. This new detection signal is immune to the thermal noise and is mainly limited by the linewidth measurement.

ACKNOWLEDGMENTS

The authors acknowledge financial support from the National Natural Science Foundation of China under Grant Nos. 11004003, 11121091, and 11023003. Y.F.X. was also supported by the Research Fund for the Doctoral Program of Higher Education (No. 20090001120004). X.Y. was supported by the National Fund for Fostering Talents of Basic Science (Nos. J1030310 and J1103205) and the Chun-Tsung Scholar Fund for Undergraduate Research of Peking University.

[1]F. Vollmer, D. Braun, A. Libchaber, M. Khoshsima, I. Teraoka, and S. Arnold, Appl. Phys. Lett. **80**, 4057 (2002).
[2]J. L. Nadeau, V. S. Iltchenko, D. Kossakovski, G. H. Bearman, and L. Maleki, Proc. SPIE **4629**, 172 (2002).
[3]E. Krioukov, J. Greve, and C. Otto, Sens. Actuators B **90**, 58 (2003).
[4]Y.-F. Xiao, C.-L. Zou, B.-B. Li, Y. Li, C.-H. Dong, Z.-F. Han, and Q. Gong, Phys. Rev. Lett. **105**, 153902 (2010).
[5]M. Noto, M. Khoshsima, D. Keng, I. Teraoka, V. Kolchenko, and S. Arnold, Appl. Phys. Lett. **87**, 223901 (2005).
[6]I. M. White, H. Oveys, and X. Fan, Opt. Lett. **31**, 1319 (2006).
[7]P. Zijlstra, K. L. van der Molen, and A. P. Mosk, Appl. Phys. Lett. **90**, 161101 (2007).
[8]A. Francois and M. Himmelhaus, Appl. Phys. Lett. **92**, 141107 (2008).
[9]J. T. Robinson, L. Chen, and M. Lipson, Opt. Express **16**, 4296 (2008).
[10]H. C. Ren, F. Vollmer, and S. Arnold, Opt. Express **15**, 17410 (2007).
[11]F. Vollmer, S. Arnold, and D. Keng, Proc. Natl. Acad. Sci. U.S.A. **105**, 20701 (2008).
[12]T. Lu, H. Lee, T. Chen, S. Herchak, J.-H. Kim, S. E. Fraser, R. C. Flagan, and K. Vahala, Proc. Natl. Acad. Sci. U.S.A. **108**, 5976 (2011).
[13]J. Zhu, S. K. Ozdemir, Y.-F. Xiao, L. Li, L. He, D.-R. Chen, and L. Yang, Nat. Photonics **4**, 46 (2010).
[14]X. Yi, Y.-F. Xiao, Y.-C. Liu, B.-B. Li, Y.-L. Chen, Y. Li, and Q. Gong, Phys. Rev. A **83**, 023803 (2011).
[15]J. Knitte, T. G.McRae, K. H. Lee, and W. P. Bowen, Appl. Phys. Lett. **97**, 123704 (2010).
[16]I. Teraoka and S. Arnold, J. Opt. Soc. Am. B **26**, 1321 (2009).
[17]Y. Shen and J.-T. Shen, Phys. Rev. A **85**, 013801 (2012).
[18]J. Wiersig, Phys. Rev. A **84**, 063828 (2011).
[19]X. Yi, Y.-F. Xiao, Y. Li, Y.-C. Liu, B.-B. Li, Z.-P. Liu, and Q. Gong, Appl. Phys. Lett. **97**, 203705 (2010).
[20]L. He, S. K. Ozdemir, J. Zhu, and L. Yang, Appl. Phys. Lett. **96**, 221101 (2010).
[21]F. Vollmer and S. Arnold, Nat. Methods **5**, 591 (2008).
[22]X. Fan, I. M. White, S. I. Shopova, H. Zhu, J. D. Suter, and Y. Sun, Anal. Chim. Acta **620**, 8 (2008).
[23]J. Zhu, S. K. Ozdemir, L. He, and L. Yang, Opt. Express **18**, 23535 (2010).
[24]W. Kim, S. K. Ozdemir, J. Zhu, L. He, and L. Yang, Appl. Phys. Lett. **97**, 071111 (2010).
[25]D. S. Weiss, V. Sandoghdar, J. Hare, V. Lefèvre-Seguin, J.-M. Raimond, and S. Haroche, Opt. Lett. **20**, 1835 (1995).
[26]A. Mazzei, S. Götzinger, L. de S. Menezes, G. Zumofen, O. Benson, and V. Sandoghdar, Phys. Rev. Lett. **99**, 173603 (2007).
[27]K. R. Hiremath and V. N. Astratov, Opt. Express **16**, 5421 (2008).
[28]T. J. Kippenberg, A. L. Tchebotareva, J. Kalkman, A. Polman, and K. J. Vahala, Phys. Rev. Lett. **103**, 027406 (2009).
[29]B. Koch, Y. Yi, J.-Y. Zhang, S. Znameroski, and T. Smith, Appl. Phys. Lett. **95**, 201111 (2009).
[30]L. Deych and J. Rubin, Phys. Rev. A **80**, 061805(R) (2009).
[31]J. Kalia and R.T. Raines, Curr. Org. Chem. **14**, 138 (2010).
[32]H. K. Hunt, C. Soteropulos, and A. M. Armani, Sensor **10**, 9317 (2010).
[33]L. Bongini, D. Fanelli, F. Piazza, P. De Los Rios, S. Sandin, and U. Skoglund, Proc. Natl. Acad. Sci. U.S.A. **101**, 6466 (2004).
[34]A. M. Armani, R. P. Kulkarni, S. E. Fraser, R. C. Flagan, and K. J. Vahala, Science **317**, 783 (2007).
[35]S. A. Wise and R. A. Watters, "Bovine serum albumin (7% Solution) (SRM 927d)," NIST Gaithersburg, MD (2006).
[36]W. Kim, S. K. Özdemir, J. Zhu, and L. Yang, Appl. Phys. Lett. **98**, 141106 (2011).
[37]S. Arnold, D. Keng, S. I. Shopova, S. Holler, W. Zurawsky, and F. Vollmer, Opt. Express **17**, 6230 (2009).
[38]J. Zhu, S. K. Ozdemir, L. He, D.-R. Chen, and L. Yang, Opt. Express, **19**, 16195 (2011).